Original Article

Alpha-synuclein expression in oxytocin neurons of young and old bovine brains

Yvan Bienvenu NIYONZIMA[1)], Yuuki ASATO[1)] and Hiroya KADOKAWA[1)]

[1)] Faculty of Veterinary Medicine, Yamaguchi University, Yamaguchi-shi, Yamaguchi-ken 1677-1, Japan

Tel.: + 81 83 9335825; Fax: +81 83 9335938

Correspondence: Hiroya Kadokawa (e-mail: hiroya@yamaguchi-u.ac.jp)

Faculty of Veterinary Medicine, Yamaguchi University, Yamaguchi-shi, Yamaguchi-ken 1677-1, Japan

Tel.: + 81 83 9335825; Fax: +81 83 9335938

Running head: Alpha synuclein in oxytocin neurons

Abstract.

Understanding of central nervous system mechanisms underlying age-related infertility remains limited. Fibril α-synuclein, distinct from its monomeric form, is implicated in age-related diseases. Notably, fibril α-synuclein spreads among neurons, similar to prions, from damaged old neurons in cortex and hippocampus to healthy neurons. However, less is known whether α-synuclein propagates into oxytocin neurons, which play crucial roles in reproduction. We compared α-synuclein expression in the oxytocin neurons in suprachiasmatic nucleus (SCN), supraoptic nucleus (SON), paraventricular hypothalamic nucleus (PVN), and posterior pituitary (PP) gland of healthy heifers and aged cows to determine its role in age-related infertility. We analyzed mRNA and protein expression, along with Congo red histochemistry and fluorescent immunohistochemistry for oxytocin and α-synuclein, followed by confocal microscopy with Congo red staining. Both mRNA and protein expressions of α-synuclein were confirmed in the bovine cortex, hippocampus, SCN, SON, PVN, and PP tissues. Significant differences in α-synuclein mRNA expressions were observed in the cortex and hippocampus between young heifers and old cows. Western blots showed five bands of α-synuclein, probably reflecting monomers, dimers, and oligomers, in the cortex, hippocampus, SCN, SON, PVN, and PP tissues, and there were significant differences in some bands between the young heifers and old cows. Bright-field and polarized light microscopy did not detect obvious amyloid deposition in the aged hypothalami; however, higher-sensitive confocal microscopy unveiled strong positive signals for Congo red and α-synuclein in oxytocin neurons in the aged hypothalami. α-synuclein was expressed in oxytocin neurons, and some differences were observed between young and old hypothalami.

Keywords: Ageing, Paraventricular hypothalamic nucleus, Posterior pituitary gland, Suprachiasmatic nucleus, Supraoptic nucleus

Introduction

Aging increases the risk of various health problems, including infertility in both humans [1-3] and cattle [4, 5]. However, little is known about the central nervous system (CNS) mechanisms pertaining to this phenomenon. Oxytocin is a pleiotropic peptide hormone with broad implications in general health, adaptation, development, behavior, and reproduction [6]. The cell bodies of oxytocin neurons are located in the suprachiasmatic nucleus (SCN), supraoptic nucleus (SON), and paraventricular hypothalamic nucleus (PVN), and their fibers project to various brain regions (to secrete oxytocin as neurotransmitter) or to the posterior pituitary (PP) gland (to secrete oxytocin as hormone into the blood) [7]. Oxytocin is a potential therapeutic target for brain diseases such as Alzheimer's disease and Parkinson's disease in the elderly [7]. However, there is limited knowledge regarding how these neurons change with age.

α-synuclein is a protein encoded by the *SNCA* gene, and is synthesized as the brain advances from the fetal to mature stage [8-10]. Although the precise physiological functions and roles of native monomeric α-synuclein remain unclear [10], it has been observed to associate with synaptic vesicles [9] and interacts with the ATP synthase subunit to enhance ATP synthase efficiency and mitochondrial function [11]. The monomers of α-synuclein aggregate into fibril α-synuclein, which causes brain diseases with advancing age, including Alzheimer’s disease, Parkinson's disease, and Lewy body dementia [12-14]. Moreover, the interaction of α-synuclein oligomers with ATP synthase switches its role from physiological to pathological, resulting in mitochondrial dysfunction [11]. Furthermore, aggregated α-synuclein damages cells [12] and lipid rafts in the plasma membrane [15]. Importantly, similar to prions, α-synuclein propagates among neurons in the cortex and hippocampus [16]. However, no studies have investigated whether α-synuclein propagates to hypothalamic oxytocin neurons or whether infected oxytocin neurons synthesize α-synuclein.

Aged brains have amyloid deposits due to various causative molecules, including amyloid-β and α-synuclein [17, 18]. The traditional method for visualizing amyloid deposition due to various causative molecules is Congo red staining for bright-field and polarized light microscopy (green, yellow, orange, or red) [19]. However, recent studies have reported that Congo red-positive regions can be detected by

higher-sensitivity confocal microscopy [20-22]. Amyloid deposition is thought to occur only in the extracellular space. However, a recent study on Lewy body dementia revealed that amyloid deposition can also occur in the cytoplasm [23]. Congo red fluorescence is also detected inside the neurons using by fluorescence microscopy [24]. However, little is known regarding amyloid deposition in the hypothalamus. Interestingly, the intra-cerebro-ventricular injection of aggregated amyloid β fragment may damage hypothalami in rats [25], meaning that oxytocin neurons may be affected by amyloid deposition.

To the best of our knowledge, no previous study has reported the expression of α-synuclein in oxytocin neurons and how this expression differs between young and old hypothalami. Therefore, we compared α-synuclein expression in the oxytocin neurons of SCN, SON, PVN, and PP between healthy heifers and old cows to estimate the importance of α-synuclein in aging-related infertility.

Materials and Methods

Animals and treatments

All experiments were performed in accordance with the Guiding Principles for the Care and Use of Experimental Animals in the Field of Physiological Sciences (Physiological Society of Japan) and approved by the Committee on Animal Experiments of Yamaguchi University (approval number 301).

All cattle were managed by our contracted farmer in western Japan. The farm had open free-stall barns with free access to water. The cattle were fed twice daily with a total mixed ration according to the Japanese feeding standard [26]. All cattle were non-lactating, non-pregnant, and with no follicular cysts, luteal cysts, or other ovarian disorders, as observed based on macroscopic examinations of the ovaries [27]. Japanese Black heifers mature sexually at about 15 months [28].

We obtained brain samples (cortex, hippocampus, anterior hypothalamus containing the SCN and SON [‘S & S’ block], and posterior hypothalamus containing the PVN and SON [‘P & S’ block]) from healthy post-pubertal Japanese Black heifers (23.0 ± 1.4 months of age; n = 5; young group) and old Japanese Black cows (162.8 ± 5.7 months of age; n = 5; old group) using methods detailed in our

previous studies. [29-31] and in Supplementary Figure 1. The frontal lobe cortex was collected caudal to the central sulcus near the midline. The hippocampus was collected from the temporal lobe, ventral to the lateral ventricle, after identification based on its unique shape [32]. Old cows were slaughtered after completing sufficient parturition time, usually after 10 years of age, as planned by the farmers, to obtain beef. Each block was stored in 4% paraformaldehyde at 4°C for 24 h. The fixed blocks were placed in a 20% sucrose solution at 4°C for 72 h. They were then stored in 30% sucrose solution at 4°C until the block was submerged for at least 48 h.

We also collected cortex, hippocampus, PP, S & S, and P & S tissue samples from other healthy post-pubertal Japanese Black heifers (22.5 ± 1.3 months of age; n = 6; young group) and old Japanese Black cows (160.7 ± 10.8 months of age; n=6; old group) to perform reverse transcription-polymerase chain reaction (RT-PCR), quantitative RT-PCR, or western blotting. Both S & S and P & S blocks were cut along their midlines to obtain the left and right sides. Using the bovine brain atlas [33, 34] as a reference, the blocks were cut based on their exterior shapes, with the third or lateral ventricles as landmarks. The tissues were immediately frozen in liquid nitrogen and stored at −80 °C until RNA or protein extraction.

RT-PCR, sequencing of amplified products, and homology search in gene databases

Total RNA was extracted from the samples of cortex, hippocampus, S & S, P & S, and PP tissues (n=6 per group per region) using RNAzol RT isolation reagent (Molecular Research Centre Inc., Cincinnati, OH, USA). The extracted RNA samples were treated with a ribonuclease-free deoxyribonuclease (Toyobo, Tokyo, Japan). The concentration and purity of each RNA sample were evaluated to ensure the A_{260}/A_{280} nm ratio was in the acceptable range of 1.8–2.1. The mRNA quality of all samples was verified by electrophoresis of total RNA, and the 28S:18S ratios were 2:1. The complementary deoxyribonucleic acid (cDNA) was synthesized using the Verso cDNA Synthesis Kit (Thermo Fisher Scientific, Waltham, MA, USA).

PCR was conducted using primers designed using the Primer3 algorithm based on the reference sequences of bovine *SNCA* (National Center for Biotechnology Information [NCBI] reference sequence of bovine *SNCA* is NM_001034041.2). Supplementary Table 1 shows the details of the primers. The

PCR was performed using 50 ng of cDNA and polymerase (Tks Gflex DNA Polymerase, Takara Bio Inc., Shiga, Japan) under the following thermocycles: 94°C for 1 min for pre-denaturing followed by 35 cycles of 98°C for 10 sec, 60°C for 15 sec, and 68°C for 30 sec. PCR products were separated on 1.5% agarose gel by electrophoresis with a molecular marker (Gene Ladder 100 [0.1-2kbp], Nippon Gene, Tokyo, Japan). The PCR products were sequenced with a sequencer (ABI3130, Thermo Fisher Scientific) using one of the PCR primers. The sequences obtained were used as query terms to search the homology sequence in the NCBI data bank using the basic nucleotide local alignment search tool (BLAST) optimized for highly similar sequences.

Quantitative RT-PCR for SNCA

After preparation of high-quality total RNA and cDNA synthesis using the previously described protocol, *SNCA* mRNA expression in young and old cortex, hippocampus, S & S, P & S, and PP tissues were compared between the young and old groups via quantitative RT-PCR as described previously [35]. The expression of each enzyme was normalized to the geometric mean of the expression of two house-keeping genes, *tyrosine 3-monooxygenase/tryptophan 5-monooxygenase activation protein zeta* (*YWHAZ*; NCBI reference sequence, NM_174814.2) and *succinate dehydrogenase complex flavoprotein subunit A* (*SDHA*; NCBI reference sequence, NM_174178.2). These two housekeeping genes are the most stable and reliable housekeeping genes to use in the bovine hypothalamus [35], and the cortex and hippocampus of sheep and rats [36, 37].

The amount of gene expression was measured in duplicate by quantitative RT-PCR with 50 ng cDNA using the CFX96 Quantitative RT-PCR System (Bio-Rad, Hercules, CA, USA) and Power SYBR Green PCR Master Mix (Thermo Fisher Scientific), together with a 6-point relative standard curve, non-template control, and no reverse-transcription control. Standard 10-fold dilutions of purified and amplified DNA fragments were prepared. Temperature conditions for all genes were as follows: 95°C for 10 min for pre-denaturation; five cycles each of 95°C for 15 sec and 66°C for 30 sec; and 40 cycles each of 95°C for 15 sec and 60°C for 60 sec. Reactions with a coefficient of determination (R2) > 0.98 and efficiency between 95 and 105% were considered optimized. The coefficients of variation of quantitative RT-PCRs were less than 6%. The concentration of PCR products was calculated by

comparing the Cq values of unknown samples with the standard curve using the appropriate software (CFXmanagerV3.1, Bio-Rad). Subsequently, the *SNCA* amount was divided by the geometric mean of *YWHAZ* and *SDHA* in each sample.

Antibodies

Human/rat/mouse α-synuclein rabbit polyclonal antibody (GTX112799; GeneTex, Inc., CA, USA) recognizes human α-synuclein (NP_001029213.1). This antigen sequence had a 95% homology to bovine α-synuclein (NP_001029213.1) but no homology to other bovine proteins, as determined using protein BLAST.

We also used an anti-oxytocin mouse monoclonal antibody (clone number 4G11: MAB5296; Sigma Aldrich, St. Louis, MO, USA) raised against a synthetic oxytocin peptide, CYIQNCPLG. This sequence had a 100% homology to bovine oxytocin (NP_789825.1). This antibody was used for immunohistochemistry to visualize oxytocin neurons in the rat brain [38].

Western Blotting for α-synuclein detection

We used a previously reported method, with minor modifications, for western blotting of bovine brain [30, 31]. Briefly, proteins were extracted from the frozen stock tissues of young and old groups (n = 6 per region per group) using a tissue protein extraction reagent (T-PER; Thermo Fisher Scientific) with a Halt Protease Inhibitor Cocktail (Thermo Fisher Scientific). In addition, proteins were extracted from a whole brain of female mouse (5 weeks old, B6C3F1/Slc, Japan SLC, Inc., Shizuoka, Japan) for use as a positive control. The extracted protein samples were boiled with sample buffer solution with reducing reagent (6x) for SDS-PAGE (09499-14; Nacalai Tesque, Kyoto, Japan) at 100°C for 3 min. Protein samples (8,000 ng of total protein) were loaded onto a sodium dodecyl sulphate-polyacrylamide gel (4–15% Criterion TGX gel, Bio-Rad) alongside a molecular weight marker (Multicolor Protein Ladder; Nippon Gene Co., Ltd., Tokyo, Japan). Gels were run at 100 V for 90 min. Proteins were transferred onto polyvinylidene fluoride (PVDF) membranes by electroblotting at 1.0 A and 25 V for 30 min using the Trans-Blot Turbo system (Bio-Rad). The PVDF membranes were stained with Revert 700

total protein stain (LI-COR Biosciences, Lincoln, NE, USA) for 5 min. After two 30-s washing cycles with 30% methanol containing 6.7% acetic acid, the PVDF membranes were neutralized with 10 mM Tris–HCl (pH 7.6) and 150 mM NaCl solution. Subsequently, the membranes were scanned using an Odyssey CLx (LI-COR Biosciences) to calculate the total protein content based on the density in each lane.

The Can Get Signal Immunoreaction Enhancer kit (Toyobo Co. Ltd, Osaka, Japan) served as a blocking membrane (1 h at 25°C) for the primary antibody reaction (16 h at 4°C) with the anti-α-synuclein antibody (1:100,000 dilution in 20 ml of immunoreaction enhancer solution I supplemented with 20 μg normal goat IgG) and secondary antibody reaction (1 h at 25°C) with goat anti-rabbit IgG horseradish peroxidase-conjugated antibody (Bethyl Laboratories Inc., Montgomery, TX, USA; 1:100,000 dilution in 20 ml of immunoreaction enhancer solution II supplemented with 20 μg normal goat IgG).

Protein bands were visualized using the Amersham ECL-Prime chemiluminescence kit (Cytiva, Marlborough, MA, USA) and a CCD imaging system (Amersham Image Quant 800, Cytiva). To verify signal specificity, several negative controls were included, wherein the primary antibodies were omitted or normal rabbit IgGs were used instead of the primary antibodies. Signal specificity was also confirmed using negative controls in which the primary antibodies were pre-absorbed with 5 nM antigen peptide (Scrum Inc., Tokyo, Japan). ImageQuant TL (version 8.2; Cytiva) software was used to measure band sizes and volumes. The frequently used control proteins, such as β-actin, GAPDH, and α-tubulin, are not suitable controls for western blotting in brain research [39,40]. This study utilized the REVERT total protein stain as the loading control, which demonstrated significant advantages over housekeeping proteins [40]. Consequently, the level of α-synuclein was normalized to the total protein level.

Cryosection

After sucrose treatment, serial coronal sections were cut into 10 μm (for Congo Red staining) or 50 μm thick (for immunohistochemistry, followed by Congo red staining) sections using a cryostat based on the bovine brain atlas [33, 34]. The selected S & S tissues contained both anterior commissure or

optic chiasm, SCN was lateral to the third ventricle, and SON was medial to optic chiasm. The selected P & S tissues contained fornix, PVN was lateral to the third ventricle, and SON was lateral to the optic tract. Every sixth section of the tissue was subjected to staining for α-synuclein, oxytocin, and Congo red. The 50 μm thick sections were then stored in 25 mM PBS containing 50% glycerol, 250 mM sucrose, and 3.2 mM $MgCl_2 \cdot 6H_2O$ at –20°C until used for immunohistochemistry. The 10 μm thick sections were affixed to slide glass (MAS coat Superfrost, Matsunami-Glass, Osaka, Japan).

Congo red staining

The slides attached with 10 μm thick sections were covered in hematoxylin (New Type M, Muto Pure Chemicals Co., LTD., Tokyo, Japan) for 2 min. After washing with water, Congo red solution (New Type M; Muto Pure Chemicals Co., Ltd.) was used for staining for 3 min. The sections were rinsed by water twice and differentiated by 0.2% potassium hydroxide 80% ethanol (alkaline ethanol) for 3 sec; then, the sections were dehydrated in 70%, 90%, 100%, and 100% ethanol and cleared with three changes of xylene. After attaching coverslips, the stained sections were observed under both bright-field and polarized light using a microscope (Eclipse Si, Nikon, Tokyo, Japan).

Fluorescent immunohistochemistry and confocal microscopy

Frozen stock brain tissue was thawed and washed twice with PBS. Free-floating tissue sections were permeabilized with PBS containing 0.5% Tween 20 for 3 min. We combined two quenching methods, glycine/hydrogen peroxide [30, 31] and Vector True VIEW autofluorescence quenching (VTVAQ) kit (Vector Laboratories Inc., Burlingame, CA, USA). Briefly, the tissue was blocked with PBS containing 2% normal goat serum, 50 mM glycine, 0.05% Tween 20, 0.1% Triton X 100, and 0.1% BSA for 30 min [30]. The sections were incubated with a cocktail of primary antibodies (anti-oxytocin mouse and anti-α-synuclein rabbit antibodies [all diluted as 1:1,000]) dissolved in PBS containing 10 mM glycine, 0.05% Tween 20, 0.1% Triton X 100, and 0.1% hydrogen peroxide at 4°C for 16 h. The sections were washed once with PBS containing 0.5 % Tween 20 (PBST), and twice with PBS, the sections were incubated with a cocktail of fluorochrome-conjugated secondary antibodies (Alexa Fluor

488 goat anti-rabbit IgG, and Alexa Fluor 647 goat anti-mouse IgG [all from Thermo Fisher Scientific and diluted to 1 μg/ml]) and 1 μg/ml of 4′, 6′-diamino-2-phenylindole (DAPI; Wako Pure Chemicals) for 4 h at room temperature. Sections were washed once with PBST and twice with PBS. Each free-floating section was transferred to a slide glass. After drying overnight, the sections were stained by Congo red solution for 3 min. The sections were rinsed twice with water, differentiated by alkaline ethanol for 3 seconds, and washed by water. The sections were stained with PBS containing 1 μg/ml of DAPI again for 10 min. Subsequently, the VTVAQ kit was used according to the manufacturer's protocol. After 5 min incubation with the kit, the sections were rinsed twice with PBS and cover glass was attached using ProLong Glass Antifade Mountant (Thermo Fisher Scientific).

The sections were observed under a confocal microscope (LSM710; Carl Zeiss, Göttingen, Germany) equipped with a 405 nm diode laser, 488 nm argon laser, 533 nm HeNe laser, and 633 nm HeNe laser. Images obtained by fluorescence microscopy were scanned with a 20× or 40× oil-immersion objective and recorded with a CCD camera. Congo red staining was viewed at 546 nm using the helium-neon laser [20-22]. Oxytocin, α-synuclein, and Congo red localization were examined using confocal images of triple-labeled specimens. To verify the specificity of the signals, we included several negative controls, in which the primary antiserum was omitted or pre-absorbed with 5 nM of the antigen peptide, or in which normal rabbit IgG was used instead of the primary antibody.

We defined various segments of neurons based on the following criteria: the cell body is round or polygonal in shape with a diameter is more than 8 μm; the fiber is shown as a continuous or dotted line of immunopositive signal. We specified oxytocin neurons if they had a shape similar to that reported in a previous paper on bovine oxytocin neurons [33] and showed oxytocin-positive signals.

To evaluate co-localization, the oxytocin signal was shown in red and either α-synuclein or Congo red was shown in green. The percentage of cell bodies or fibers of oxytocin single-labeled neurons and double/triple-labeled cell bodies or fibers of neurons among all oxytocin-positive cell bodies or fibers of neurons were determined for each individual. For this purpose, we analyzed all areas of four randomly selected sections containing the SCN, four sections containing the SON, four sections containing the PVN, and twelve sections containing the PP from each individual.

Statistical analysis

Grubb's test verified the absence of outliers. The Shapiro–Wilk and Kolmogorov–Smirnov Lilliefors tests verified the normality of distribution of each variable. Two-factor analysis of variance (ANOVA) was employed to evaluate the effect of the different groups (young vs. old) on the α-synuclein band intensity in western blots. Differences in each band of α-synuclein protein intensity, total band intensity of α-synuclein, and protein or mRNA expression were analyzed using non-paired *t*-test. *T*-test was utilized to compare the young and old groups in the percentage of cell bodies or fibers of oxytocin single-labeled neurons and the percentage of double/triple-labeled cell bodies or fibers of neurons among all oxytocin-positive cell bodies or fibers of neurons in the SCN, PVN, SON, or PP tissues. The level of significance was set at $P < 0.05$. Data are expressed as the means ± standard error of the mean.

Results

Detection of α-synuclein mRNA

Agarose gel electrophoresis yielded PCR products of the expected size, indicating the presence of *α-synuclein* in the bovine cortex, hippocampus, S & S, P & S, and PP tissues (303 bp; Supplementary Figure 2). Homology searching of the obtained sequences of the amplified products in the gene databases revealed that the best match alignment was for bovine *SNCA* (NM_001034041.2). Both had a query coverage of 100%, an e-value of 0.0, and a maximum alignment identity of 99%. No other bovine genes were found to share homology with the obtained sequences of the amplified products, indicating that the sequences of the amplified products were identical to those of bovine *SNCA*.

Detection of α-synuclein protein

Western blotting confirmed the presence of α-synuclein in the young and old cortex, hippocampus, S & S, P & S, and PP tissues, with differences in intensity among sample types (Fig. 1A). The expected size of the α-synuclein monomer form was 16.6 kDa. We observed other four band sizes,

most likely dimers (36.9 kDa), oligomers (53.8 kDa, 65.2 kDa, and 91.0 kDa or 95.1 kDa). Two-factor ANOVA for band intensity after normalization to total protein intensity (Fig. 1B) revealed the significant effects of age in the cortex, S & S, P & S, and PP tissues, but not in the hippocampus (Fig.1C–G). Non-paired t-tests revealed significant differences in the 36.9-kDA band for S & S, P & S, and PP tissues, the 53.8-kDa band for PP, and the 65.2-kDa band for the hippocampus between young and old bovines. Non-paired t-tests revealed significant differences in the total band intensity of α-synuclein protein between young and old bovines.

Quantitative RT-PCR

Quantitative RT-PCR revealed significant differences in *SNCA* mRNA (Fig. 2) expression levels between young and old bovines in the cortex and hippocampus, but not in S & S, P & S, or PP tissues.

Congo red staining for amyloid deposit

Congo red staining coupled with bright-field microscopy displayed red or orange hues in the SCN, SON, and PVN of the old group, but not in the young group (Supplementary Figure 3). Some stained cell bodies formed clusters. Polarized light microscopy revealed red- or brown-colored cell bodies and fibers in the SCN, SON, and PVN of the old group.

Fluorescence analysis of α-synuclein and Congo red in the cortex and hippocampus

Fluorescence immunohistochemistry detected α-synuclein in the cell bodies and fibers of neurons in the cortex and hippocampus of both young and old groups (Supplementary Figure 4). Strong Congo red fluorescence was detected in the cortex and hippocampus of old group, whereas weak fluorescence was detected in young group.

Fluorescence analysis of oxytocin, α-synuclein, and Congo red

Immunofluorescence immunohistochemistry followed by Congo red staining detected α-synuclein in most of the oxytocin neuron cell bodies and fibers in the SCN (Fig. 3), SON (Fig. 4), PVN

(Fig. 5), and PP tissues (Fig. 6) in the old group, but not in the young group. Triple-positive (oxytocin-positive, α-synuclein-positive, and Congo red-positive) cell bodies and fibers were abundant in the old SCN, SON, PVN, and PP, but not in young ones. However, weak α-synuclein was solely observed occasionally in the young group (Fig. 4E, 5E, 6A, 6C). The α-synuclein-positive cell bodies of oxytocin neurons were observed in close proximity (within 5 μm) to cell bodies of other oxytocin neurons in the SCN (Fig. 3B, 3D, 3F), SON (Fig. 4B, 4D), and PVN (Fig. 5B, 5D). Strong Congo red fluorescence was detected in the SCN, SON, PVN, and PP of the old group. In contrast, only weak Congo red fluorescence was detected in the SCN, SON, PVN, and PP of the young group. Importantly, α-synuclein-positive oxytocin fibers were observed very close to a blood vessel (Fig. 6B, 6D).

Supplementary Table 2 presents the number of examined oxytocin-positive, α-synuclein-positive, and Congo red-positive cell bodies and fibers in the SCN, SON, PVN, or PP. As illustrated in Supplementary Table 3, the vast majority of cell bodies and fibers of oxytocin neurons are positive for both α-synuclein and Congo red in the SCN, SON, PVN, or PP in the old group, but not in the young group. Significant differences were evident in almost all the ratios between the two groups. In addition to oxytocin neurons, there were also α-synuclein-positive and Congo red-positive non-oxytocin neurons (as shown in Supplementary Table 3). This indicates that α-synuclein-positivity and Congo red-positivity were not exclusive to oxytocin neurons.

Discussion

The present study detected α-synuclein mRNA and protein expression in the bovine SCN, SON, PVN, and PP. Immunohistochemistry detected α-synuclein in bovine oxytocin neurons. Most of the cell bodies or fibers of oxytocin neurons were α-synuclein- and Congo red-positive were observed in the SCN, SON, PVN, and PP tissues of the old group. To the best of our knowledge, this is the first study to report α-synuclein- and Congo red-positivity in oxytocin neurons of all species. The discovered α-synuclein and Congo red positivity in SCN, SON, PVN, and PP warrant further exploration because their localization has significant implications for various physiological functions, including reproduction.

A previous study observed Congo red-positive neurons in the PVN and SON of an elderly patient

with Alzheimer's disease [41]; however, the corresponding cells were not identified. We observed strong α-synuclein and Congo red signals in the oxytocin neurons of old bovines, and positivity for both was weak in the oxytocin neurons of young bovines. It is well-known that α-synuclein monomers can combine into oligomers and fibrils, these being a driving cause of brain disease [12-14]. Monomeric α-synuclein is expressed in fetal and young healthy brains [8-10]. The western blots in this study revealed five bands, similar to those observed in a previous study on the human brain [42]. The smallest band (16.6 kDa) seemed to correspond to the monomer because the molecular weight of bovine α-synuclein is 14.5 kDa (calculated based only on the amino acid sequence [NP_001029213.1], without including the acetylation and phosphorylation sites stated in its annotation). We speculated that the second-smallest band (36.9 kDa), was a dimer, and the band intensities of old S & S, P & S, and PP tissues were significantly higher than those of the young. The band intensities of the larger bands may reflect the amount of endogenous oligomers and fibrils. A significant effect of different ages was detected by two-factor ANOVA in the cortex, S & S, P & S, and PP. Therefore, further studies are required to clarify the pathogenic roles of α-synuclein in oxytocin neurons.

As shown in Fig 6A and 6B, the oxytocin neuronal cell bodies formed clusters. A similar cluster is well known in GnRH neurons, and most GnRH neurons (86%) form multiple close appositions with dendrites of other GnRH neurons, probably for GnRH neuronal synchronization via dendrodendritic communication [43]. Therefore, oxytocin clusters may serve similar purposes. α-synuclein and Congo red positivity in oxytocin neurons may be relevant to the regulation of oxytocin secretion. It is known that α-synuclein aggregates at lipid rafts, which are important components of the plasma membrane, and inhibit cytoplasmic signaling pathways [15]. Moreover, α-synuclein behaves like prions [16]. Therefore, further studies are warranted to clarify the role of α-synuclein in the oxytocin neuron cluster.

Oxytocin neurons in the SCN, SON, and PVN project to the PP gland and secrete oxytocin into the circulating blood [7]. A previous study reported the presence of α-synuclein-positive deposits in the PP glands of the majority of elderly patients with Parkinson's disease and Lewy body dementia; however, α-synuclein-positive deposits were also present in the PP glands of elderly patients without these diseases [44]. The present study found α-synuclein signals in the fibers of oxytocin neurons very close

to blood vessels in the PP glands. Moreover, the total band intensity of α-synuclein was greater in the PP glands of older bovines than in those of younger bovines. It is known that α-synuclein is transported into and out of the brain, even via the blood-brain barrier [45]. Furthermore, amyloid deposits are reported in the hypophyses of 7-year-old cows [46]. Additionally, cultured neurons can secret α-synuclein fibrils [47]. Therefore, the findings of this study suggest another route in which α-synuclein may be secreted into the blood to suppress peripheral organs. Further studies to evaluate this hypothesis are warranted.

Similar to old human brains, old cattle brains promote amyloidosis and display Alzheimer's disease-like pathology [48]. α-synuclein contributes to the formation of amyloid deposits [17, 18]. Recent studies have reported that confocal microscopy detects the fluorescence of Congo red, and this detection has a higher sensitivity than that of traditional bright-field or polarized light microscopy [20-22]. Cytoplasmic amyloid deposits may have physiological functions, since α-synuclein interacts with and modulates the aggregation of Pmel17, a functional amyloid in melanoma [49-51]. Importantly, an oxytocin-like peptides self-assemble into amyloid fibrils [52]. Moreover, a study reported that atrial fibrillation occurs after administering a bolus of oxytocin during cesarean section [53]. Therefore, the functional amyloid concept warrants further studies for oxytocin neurons in the hypothalamus, as the present study did not provide direct evidence that α-synuclein accumulation leads to abnormal oxytocin nerve function.

This study had a limitation. The SCN, SON, and PVN specimens also contained other brain areas and nuclei because it was impossible to obtain precisely cut samples under our experimental conditions. Therefore, data from western blots and RT-PCR could not define α-synuclein expression only in oxytocin neurons. However, immunohistochemistry detected α-synuclein expression in the oxytocin neurons, which allowed us to safely conclude that bovine oxytocin neurons expressed α-synuclein.

Previous studies have clarified that the hippocampus is a unique region of the adult brain for neurogenesis [54]. We observed the highest α-synuclein expression in the hippocampus. Fetal and healthy young brains synthesize α-synuclein for an unclarified role [8, 10]. Therefore, further studies are required to clarify the roles of α-synuclein in neurogenesis. Additionally, the young cortex and

hippocampus had higher *SNCA* mRNA expression than their older counterparts. Furthermore, in a previous study [55], the levels of α-synuclein mRNA throughout the mouse brain were found to be high in young mice (2-month-old) and were observed to progressively decline in middle-aged (10-month-old) and old (20-month-old) mice. Therefore, the amounts of α-synuclein, likely the normal native monomeric α-synuclein form, appear to have declined in the brains of old cows.

Two differences in band size were observed in western blots. The largest band, measuring 95.1 kDa, was present in almost all regions except for the cortex (91.0 kDa). Second, the most prominent band was evident in the lane corresponding to the whole mouse brain. Despite extensive analyses, we were unable to ascertain the underlying mechanisms responsible for this difference. Potential explanations include differences in the chemical composition of various brain regions or inter-species variation.

In conclusion, the presence of *α-synuclein* in oxytocin neurons was demonstrated, and notable differences were observed between the hypothalamus of young and old individuals. Oxytocin plays a crucial role in supporting reproduction by promoting sexual and nursing behaviors and stimulating reproductive organs [6, 56]. Furthermore, oxytocin plays significant roles in the inhibition of age-related neurodegenerative diseases [6, 56]. Therefore, additional research is required on the mechanisms by which α-synuclein and amyloid function within the hypothalamus to influence oxytocin secretion.

Data availability

The data supporting this study will be shared upon reasonable request from the corresponding authors.

Conflict of interests

The authors have nothing to declare.

Acknowledgments

This research was partially supported by a Grant-in-Aid for Scientific Research [JSPS Kakenhi,

grant number 21H02345] from the Japan Society for the Promotion of Science (Tokyo, Japan) awarded to Hiroya Kadokawa. The funders played no role in the study design, data collection and analysis, decision to publish, or manuscript preparation. We thank Yamaguchi Prefecture (Japan) for supplying cattle brain samples. Yvan Bienvenu Niyonzima was supported by a scholarship from Japan International Cooperation Agency (Tokyo, Japan).

References

1. **Gunes S, Hekim GN, Arslan MA, Asci R**. Effects of aging on the male reproductive system. *J Assist Reprod Genet* 2016; **33**: 441-454.
2. **Van den Beld AW, Kaufman JM, Zillikens MC, Lamberts SWJ, Egan JM, van der Lely AJ.** The physiology of endocrine systems with ageing. *Lancet Diabetes Endocrinol* 2018; **6:** 647-658.
3. **Epelbaum J, Terrien J.** Mini-review: aging of the neuroendocrine system: insights from nonhuman primate models. *Prog Neuropsychopharmacol Biol Psychiatry* 2020; **100**: 109854.
4. **Osoro K, Wright IA.** The effect of body condition, live weight, breed, age, calf performance, and calving date on reproductive performance of spring-calving beef cows. *J Anim Sci* 1992; **70**:1661-1666.
5. **Malhi PS, Adams GP, Pierson RA, Singh J.** Bovine model of reproductive aging: response to ovarian synchronization and superstimulation. *Theriogenology* 2006; **66**: 1257-1266.
6. **Carter CS, Kenkel WM, MacLean EL, Wilson SR, Perkeybile AM, Yee JR, Ferris CF, Nazarloo HP, Porges SW, Davis JM, Connelly JJ, Kingsbury MA.** Is Oxytocin "Nature's Medicine"? *Pharmacol Rev* 2020; **72**: 829-861.
7. **Ghazy AA, Soliman OA, Elbahnasi AI, Alawy AY, Mansour AM, Gowayed MA**. Role of oxytocin in different neuropsychiatric, neurodegenerative, and neurodevelopmental disorders. *Rev Physiol Biochem Pharmacol* 2023; **186**: 95-134.
8. **Raghavan R, Kruijff Ld, Sterrenburg MD, Rogers BB, Hladik CL, White CL 3rd.** Alpha-synuclein expression in the developing human brain. *Pediatr Dev Pathol* 2004; **7**; 506-516.

9. **Sulzer D, Edwards RH.** The physiological role of α-synuclein and its relationship to Parkinson's Disease. *J Neurochem* 2019; **150:** 475-486.
10. **Jin M, Wang S, Gao X, Zou Z, Hirotsune S, Sun L.** Pathological and physiological functional cross-talks of α-synuclein and tau in the central nervous system. *Neural Regen Res* 2024; **19**: 855-862.
11. **Tripathi T, Chattopadhyay K.** Interaction of α-Synuclein with ATP Synthase: Switching Role from Physiological to Pathological. *ACS Chem Neurosci* 2019; **10**: 16-17.
12. **Fields CR, Bengoa-Vergniory N, Wade-Martins R.** Targeting alpha-synuclein as a therapy for Parkinson's disease. *Front Aging Neurosci* 2019; **12**: 299.
13. **Ahmed J, Fitch TC, Donnelly CM, Joseph JA, Ball TD, Bassil MM, Son A, Zhang C, Ledreux A, Horowitz S, Qin Y, Paredes D, Kumar S.** Foldamers reveal and validate therapeutic targets associated with toxic α-synuclein self-assembly. *Nature Commun* 2022; **13**: 2273.
14. **Deyell JS, Sriparna M, Ying M, Mao X.** The Interplay between α-Synuclein and Microglia in α-Synucleinopathies. *Int J Mol Sci* 2023; **24**: 2477.
15. **Perissinotto F, Stani C, De Cecco E, Vaccari L, Rondelli V, Posocco P, Parisse P, Scaini D, Legname G, Casalis L.** Iron-mediated interaction of alpha synuclein with lipid raft model membranes. *Nanoscale* 2020; **12**: 7631-7640.
16. **Melki R.** Alpha-synuclein and the prion hypothesis in Parkinson's disease. *Rev Neurol* 2018; **174**: 644-652.
17. **Yanamandra K, Gruden MA, Casaite V, Meskys R, Forsgren L, Morozova-Roche LA**. α-synuclein reactive antibodies as diagnostic biomarkers in blood sera of Parkinson's disease patients. *PLoS One* 2011; **6**: 18513.
18. **Marsh SE, Blurton-Jones M**. Examining the mechanisms that link β-amyloid and α-synuclein pathologies. *Alzheimer's Res Ther* 2012; **4**: 11.
19. **Obrenovich ME, Monnier VM**. Glycation stimulates amyloid formation. *Sci Aging Knowledge Envi* 2004; **2004**: pe3
20. **Schultz SW, Nilsson KP, Westermark GT.** Drosophila melanogaster as a model system for studies of islet amyloid polypeptide aggregation. *PLoS One* 2011; **6**: e20221.

489 **21. Scivetti M, Favia G, Fatone L, Maiorano E, Crincoli V**. Concomitant use of Congo red staining
490 and confocal laser scanning microscopy to detect amyloidosis in oral biopsy: A clinicopathological
491 study of 16 patients. *Ultrastruct Pathol* 2016; **40**: 86-91.
492 **22. Castellani C, Fedrigo M, Frigo AC, Barbera MD, Thiene G, Valente M, Adami F, Angelini A.**
493 Application of confocal laser scanning microscopy for the diagnosis of amyloidosis. *Virchows Arch*
494 2017;**470**, 455-463.
495 **23. Araki K, Yagi N, Aoyama K, Choong CJ, Hayakawa H, Fujimura H, Nagai Y, Goto Y,**
496 **Mochizuki H.** Parkinson's disease is a type of amyloidosis featuring accumulation of amyloid fibrils
497 of α-synuclein. *Proc Natl Acad Sci U S A* 2019; **116**: 17963-17969.
498 **24. Puladi B, Dinekov M, Arzberger T, Taubert M, Köhler C**. The relation between tau pathology
499 and granulovacuolar degeneration of neurons. *Neurobiol Dis* 2021; **147**: 105138.
500 **25. Zussy C, Brureau A, Delair B, Marchal S, Keller E, Ixart G, Naert G, Meunier J, Chevallier**
501 **N, Maurice T, Givalois L.** Time-course and regional analyses of the physiopathological changes
502 induced after cerebral injection of an amyloid β fragment in rats. *Am J Pathol* 2011; **179:** 315-334.
503 26. Agriculture, forestry and fisheries Research Council secretariat**.** Nutrition requirement. In: Ministry
504 of Agriculture, Forestry and Fisheries (eds.) Japanese feeding standard for beef cattle. Tokyo, Japan:
505 Central Association of Livestock, Industry; 2022: 51-72. (in Japanese)
506 **27. Kamomae H**. Reproductive disturbance. In: Nakao T, Tsumagari S, Katagiri S (eds.) Veterinary
507 Theriogenology. Tokyo, Japan: Buneidou Press; 2012: 283-340. (in Japanese)
508 **28. Inoue K, Hosono M, Oyama H, Hirooka H.** Genetic associations between reproductive traits for
509 first calving and growth curve characteristics of Japanese Black cattle. *Anim Sci J* 2020; **91**,
510 e13467.
511 **29. Kadokawa H, Pandey K, Nahar A, Nakamura U, Rudolf FO.** Gonadotropin-releasing hormone
512 (GnRH) receptors of cattle aggregate on the surface of gonadotrophs and are increased by elevated
513 GnRH concentrations. *Anim Reprod Sci* 2014; **150:** 84–95.
514 **30. Kereilwe O, Kadokawa H.** Anti-Müllerian hormone and its receptor are detected in most
515 gonadotropin-releasing-hormone cell bodies and fibers in heifer brains. *Domest Anim Endocrinol*
516 2020; **72:** 106432.

517 **31. Kereilwe O, Kadokawa H.** Decreased Anti-Müllerian hormone and Anti-Müllerian hormone
518 receptor type 2 in hypothalami of old Japanese Black cows. *J Vet Med Sci* 2020; **82**: 1113-1117.
519 doi:10.1292/jvms.20-0159.
520 **32. Rech R, Giaretta PR, Corrie B, de Barros CS.** Gross and histopathological pitfalls found in the
521 examination of 3,338 cattle brains submitted to the BSE surveillance program in Brazil. *Pesquisa*
522 *Veterinária Brasileira* 2018;**38**, 2099-2108.
523 **33. Graïc JM, Corain L, Peruffo A, Cozzi B, Swaab DF.** The bovine anterior hypothalamus:
524 Characterization of the vasopressin-oxytocin containing nucleus and changes in relation to sexual
525 differentiation. *J Comp Neurol* 2018; **526**: 2898-2917.
526 34. **Okamura H.** Brain atlas of cattle. In: Agriculture, Forestry and Fisheries Research Council (eds.)
527 A foundational research for elucidation and estimation. Tokyo, Japan: Ministry of Agriculture,
528 Forestry and Fisheries. 2002: 41–72. (in Japanese)
529 **35. Kadokawa H, Kotaniguchi M, Kereilwe O, Kitamura S.** Reduced gonadotroph stimulation by
530 ethanolamine plasmalogens in old bovine brains. *Sci Rep* 2021; **11**: 4757.
531 **36. Bonefeld BE, Elfving B, Wegener G.** Reference genes for normalization: a study of rat brain tissue.
532 *Synapse* 2008; **62**: 302-309.
533 **37. Gossner AG, Foster JD, Fazakerley JK, Hunter N, Hopkins J.** Gene expression analysis in
534 distinct regions of the central nervous system during the development of SSBP/1 sheep scrapie. *Vet*
535 *Microbiol* 2011; **147**: 42-48.
536 **38. Dabrowska J, Hazra R, Ahern TH, Guo JD, McDonald AJ, Mascagni F, Muller JF, Young LJ,**
537 **Rainnie DG.** Neuroanatomical evidence for reciprocal regulation of the corticotrophin-releasing
538 factor and oxytocin systems in the hypothalamus and the bed nucleus of the stria terminalis of the
539 rat: Implications for balancing stress and affect. *Psychoneuroendocrinology* 2011; **36**: 1312-1326.
540 39. **Goasdoue K, Awabdy D, Bjorkman ST, Miller S.** Standard loading controls are not reliable for
541 Western blot quantification across brain development or in pathological conditions. *Electrophoresis*
542 2016; **37**: 630-634.
543 40. **Kirshner ZZ, Gibbs RB.** Use of the REVERT® total protein stain as a loading control
544 demonstrates significant benefits over the use of housekeeping proteins when analyzing brain

545 homogenates by Western blot: An analysis of samples representing different gonadal hormone states.
546 *Mol Cell Endocrinol*. 2018; **473**: 156-165.
547 **41. Simpson J, Yates CM, Watts AG, Fink G.** Congo red birefringent structures in the hypothalamus
548 in senile dementia of the Alzheimer type. *Neuropathol Appl Neurobiol* 1988; **14:** 381-393.
549 **42. Tong J, Wong H, Guttman M, Ang LC, Forno LS, Shimadzu M, Rajput AH, Muenter MD,**
550 **Kish SJ, Hornykiewicz O, Furukawa Y**. Brain alpha-synuclein accumulation in multiple system
551 atrophy, Parkinson's disease and progressive supranuclear palsy: a comparative investigation. *Brain*
552 2010; **133:** 172-188.
553 **43. Campbell RE, Gaidamaka G, Han SK, Herbison AE.** Dendro-dendritic bundling and shared
554 synapses between gonadotropin-releasing hormone neurons. *Proc Natl Acad Sci U S A* 2009; **106**:
555 10835-10840.
556 **44. Homma T, Mochizuki Y, Mizutani T.** Phosphorylated α-synuclein immunoreactivity in the
557 posterior pituitary lobe. *Neuropathology* 2012; **32**: 385-389.
558 **45. Sui YT, Bullock KM, Erickson MA, Zhang J, Banks WA**. Alpha synuclein is transported into and
559 out of the brain by the blood-brain barrier. *Peptides* 2014; **62**: 197-202.
560 **46. Yamada M, Kotani Y, Nakamura K, Kobayashi Y, Horiuchi N, Doi T, Suzuki S, Sato N, Kanno**
561 **T, Matsui T.** Immunohistochemical distribution of amyloid deposits in 25 cows diagnosed with
562 systemic AA amyloidosis. *J Vet Med Sci* 2006; **68**: 725-729.
563 **47. Gegg ME, Verona G, Schapira AHV.** Glucocerebrosidase deficiency promotes release of α-
564 synuclein fibrils from cultured neurons. *Hum Mol Genet* 2020; **29:** 1716-1728.
565 *48.* **Moreno-Gonzalez I, Edwards G 3rd, Morales R, Duran-Aniotz C, Escobedo G Jr, Marquez**
566 **M, Pumarola M, Soto C.** Aged cattle brain displays Alzheimer's disease-likepathology and
567 promotes brain amyloidosis in a transgenic animal model. *Front Aging Neurosci* 2022; **13,** 815361.
568 **49. Fowler DM, Koulov AV, Alory-Jost C, Marks MS, Balch WE, Kelly JW.** Functional amyloid
569 formation within mammalian tissue. *PLoS Biol* 2006; **4**: e6.
570 **50. Sergeeva AV, Galkin AP.** Functional amyloids of eukaryotes: criteria, classification, and biological
571 significance. *Curr Genet* 2020; **66:** 849-866.
572 **51. Dean DN, Lee JC.** Linking Parkinson's disease and melanoma: Interplay between α-Synuclein and

Pmel17 amyloid formation. *Mov Disord* 2021; **36**: 1489-1498.

52. Gobeaux F, Wien F. Reversible assembly of a drug peptide into amyloid fibrils: A dynamic circular dichroism study. *Langmuir* 2018; **34**: 7180-7191

53. Guimarães D, Windels A, Fernandes P, Chumela T. Atrial fibrillation after a bolus of oxytocin during an urgent caesarean section. *Anaesth Rep* 2023; **11**; e12214.

54. Gonçalves JT, Schafer ST, Gage FH. Adult neurogenesis in the hippocampus: From stem cells to behavior. *Cell* 2016; **167**: 897-914.

55. Mak SK, McCormack AL, Langston JW, Kordower JH, Di Monte DA. Decreased alpha-synuclein expression in the aging mouse substantia nigra. *Exp Neurol* 2009; **220**, 359-365.

56. **Buemann B**. Does activation of oxytocinergic reward circuits postpone the decline of the aging brain? *Front Psychol* 2023; **14**: 1250745.

586 **Figure Legends**

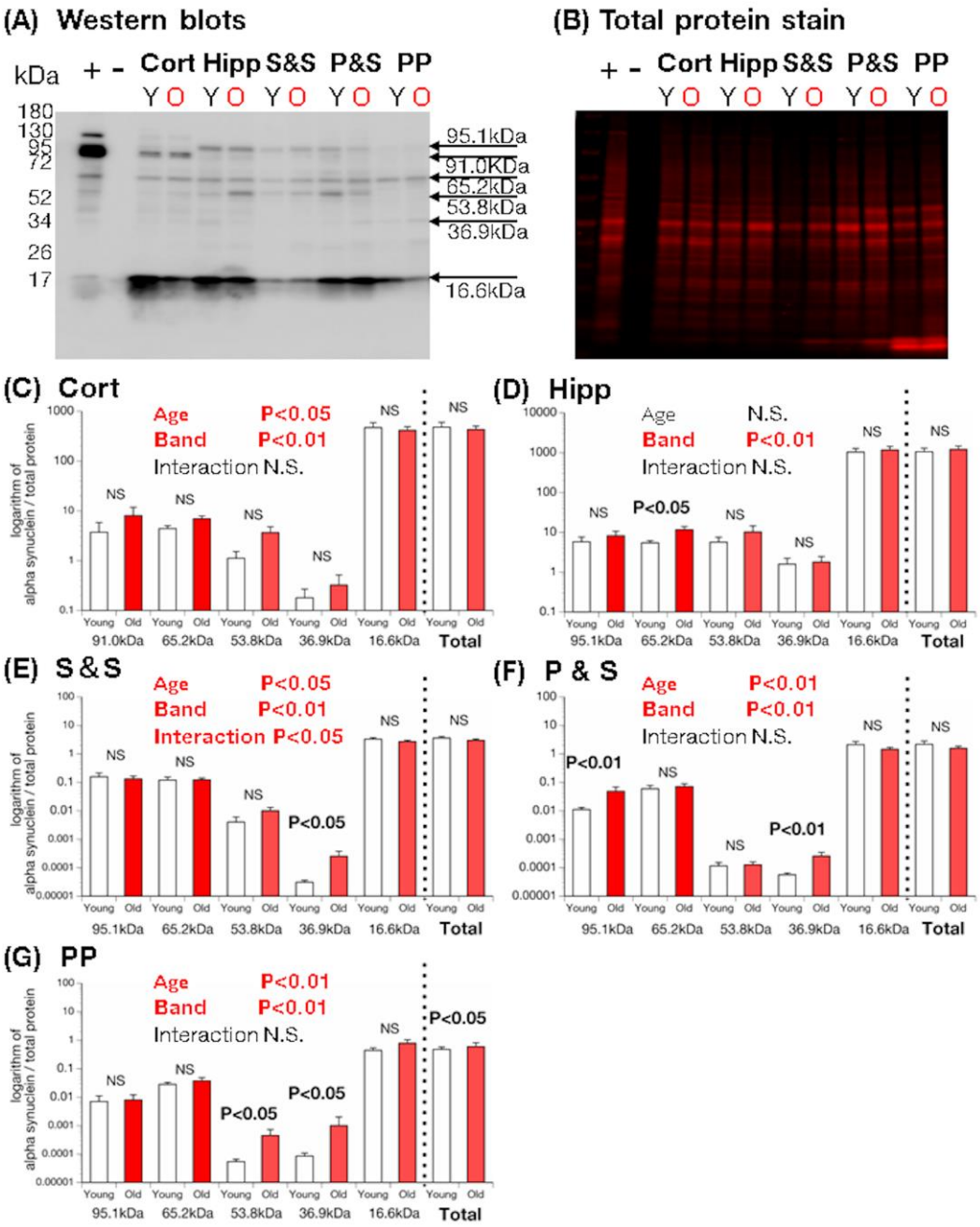

587

588 **Fig. 1.** Western blot analysis of α-synuclein in brain sections: positive control (+, whole mouse brain),
589 negative control (-, buffer only), cortex (Cort), hippocampus (Hipp), suprachiasmatic nucleus and
590 supraoptic nucleus (S & S), paraventricular hypothalamic nucleus and supraoptic nucleus (P & S), and
591 posterior pituitary (PP) tissues from post-pubertal heifers (Y; $n = 6$) and older cows (O; $n = 6$), detected
592 with anti-α-synuclein antibody (A). Representative photos of membrane stained by Revert 700 total

593 protein stain (B). Relative α-synuclein protein levels normalized to the amount of total protein based on
594 all densities in each lane (C, D, E, F, and G). Headings indicate the results of the two-way ANOVA. P-
595 values indicate significant differences by t-test between the young and old specimens.
596 ANOVA: analysis of variance
597 N.S.: non-significant
598

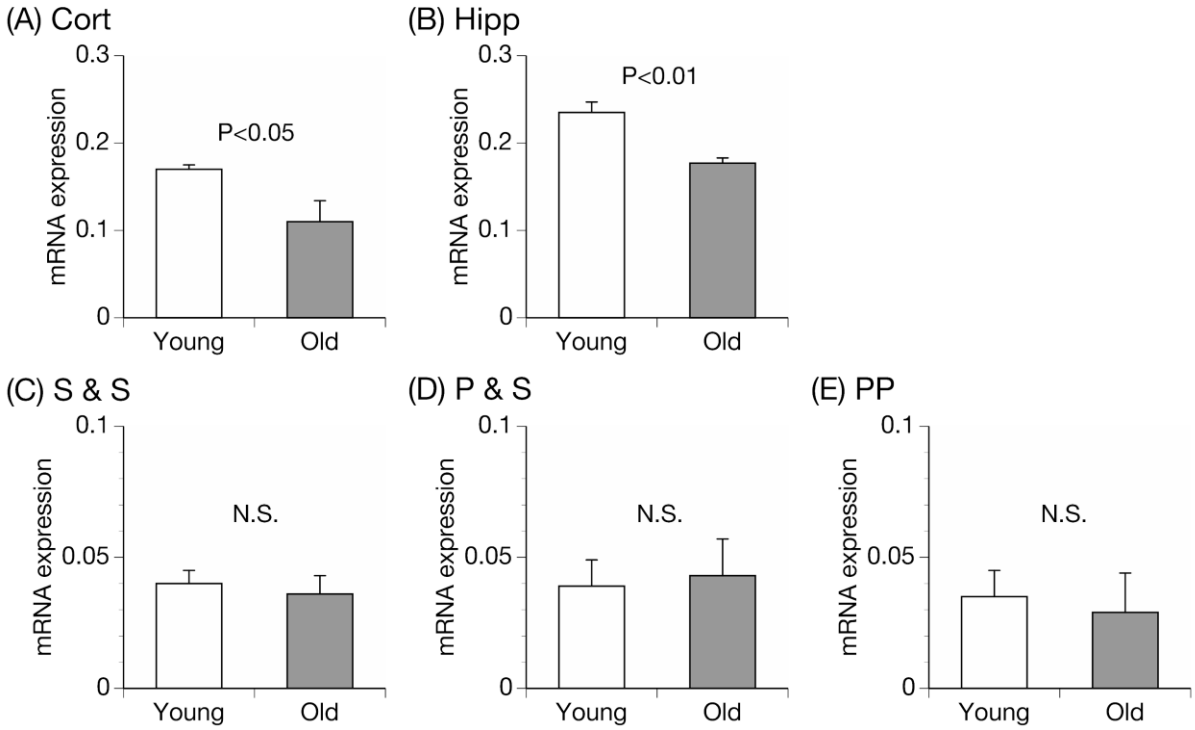

599

600

601 **Fig. 2**. Relative SNCA mRNA levels, presented as mean ± SEM, in various brain regions: cortex (Cort)
602 (A), hippocampus (Hipp) (B), suprachiasmatic nucleus and supraoptic nucleus (S & S) tissue (C),
603 paraventricular hypothalamic nucleus and supraoptic nucleus (P & S) tissue (D), and posterior pituitary
604 (PP) tissue (E), comparing healthy, post-pubertal, growing, nulliparous heifers (young group; n = 6) to
605 old, multiparous cows (old group; n = 6), as measured by RT-qPCR. Data were normalized to the
606 geometric means of *YWHAZ* and *SDHA* levels. The P-values in the upper of each graph represent the
607 results of non-paired t-test.
608 RT-qPCR: quantitative reverse transcription-polymerase chain reaction
609 SEM: standard error of mean
610 N.S.: non-significant
611

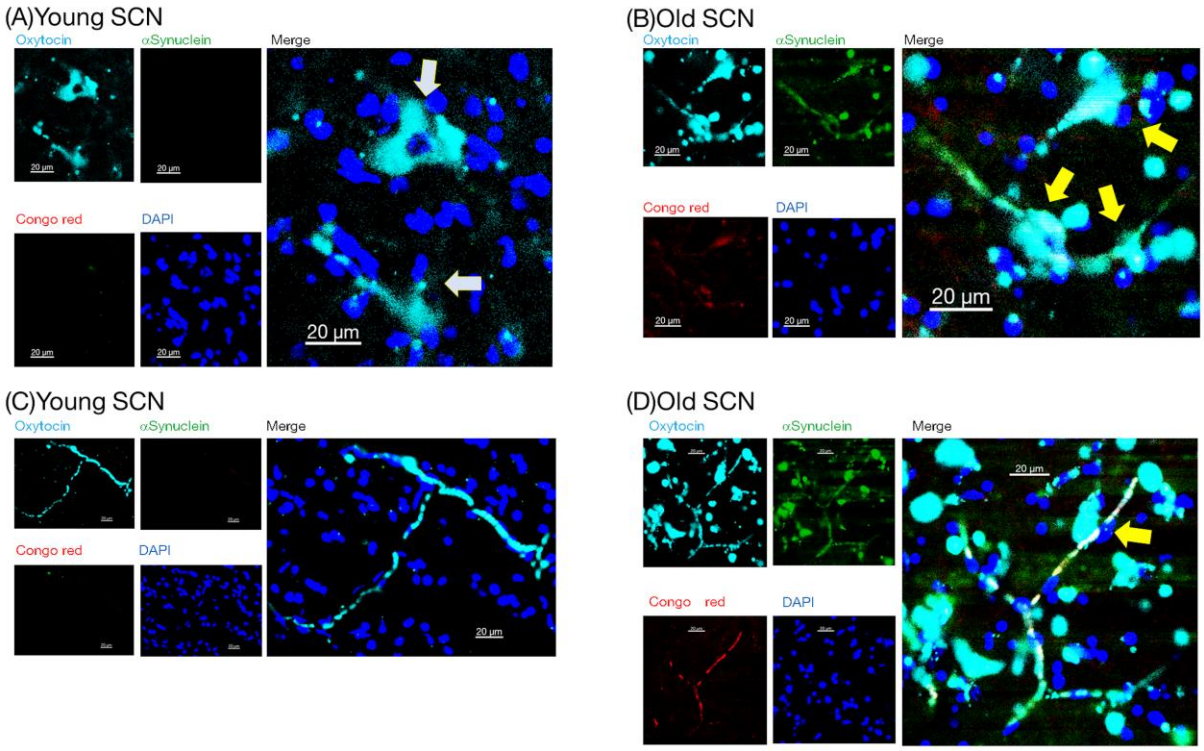

612

613 **Fig. 3.** Fluorescence photomicrographs of oxytocin, α-synuclein, Congo red, and DAPI in the SCN of
614 young and old bovines. Images were captured with laser confocal microscopy for oxytocin (light blue),
615 α-synuclein (green), Congo red (red), and DAPI (blue). In the merged photos, the yellow arrows and
616 yellow star indicate the cell body and blood vessel. Scale bars, 20 μm.
617 SCN: suprachiasmatic nucleus

618

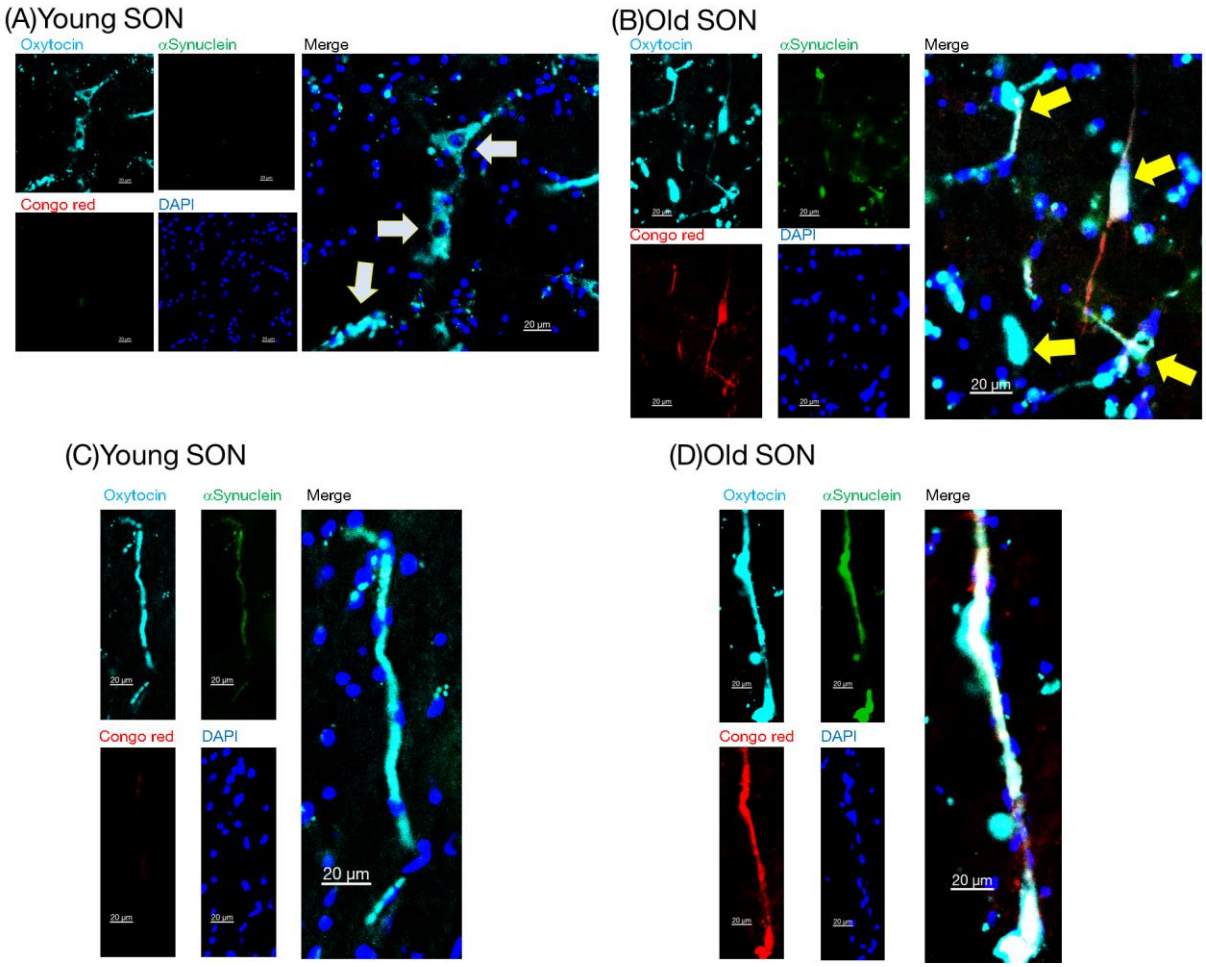

Fig. 4. Fluorescence photomicrographs of oxytocin, α-synuclein, Congo red, and DAPI in the SON of young and old bovines. Images were captured with laser confocal microscopy for oxytocin (light blue), α-synuclein (green), Congo red (red), and DAPI (blue). In the merged photos, the arrows indicate the cell body. Scale bars, 20 μm.

SON: supraoptic nucleus

627

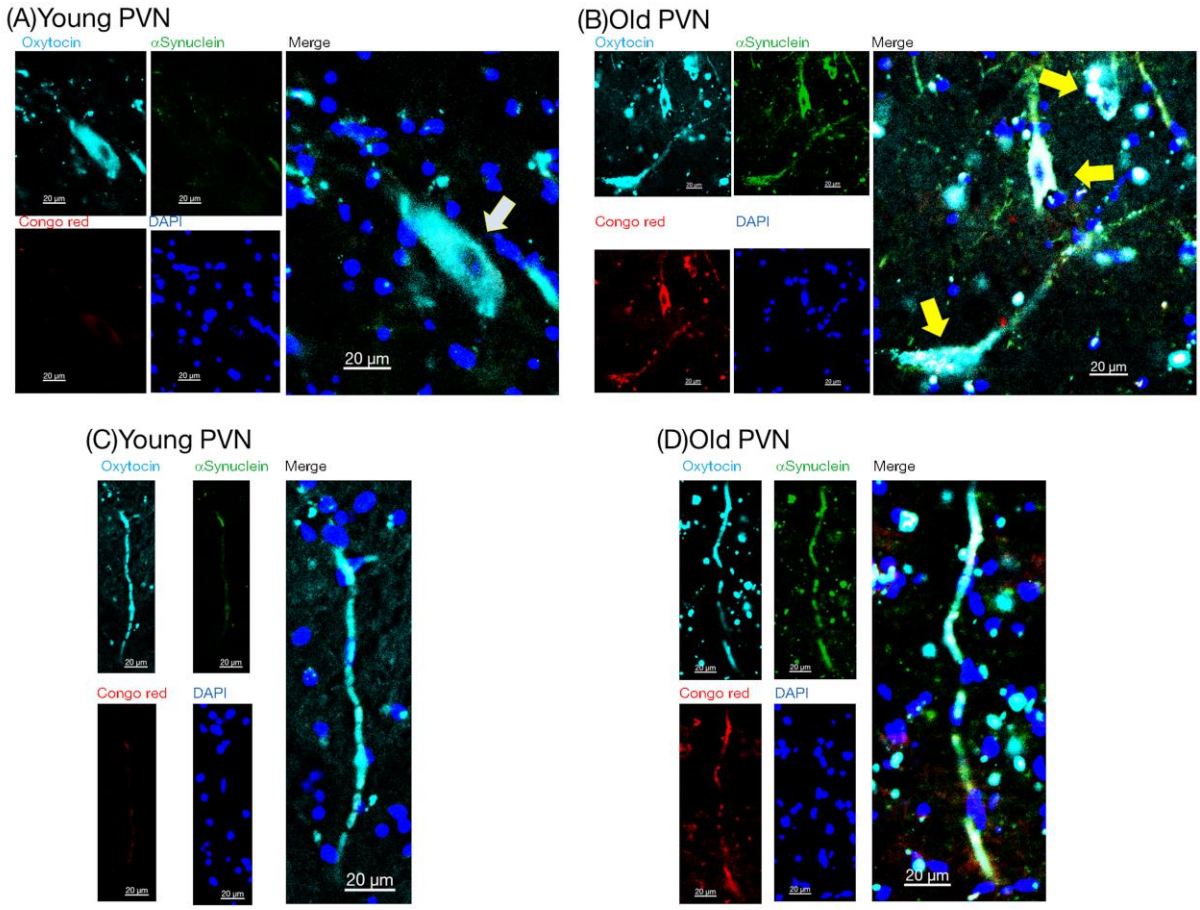

628

629 **Fig. 5.** Fluorescence photomicrographs of oxytocin, α-synuclein, Congo red, and DAPI in the PVN of

630 young and old bovines. Images were captured with laser confocal microscopy for oxytocin (light blue),

631 α-synuclein (green), Congo red (red), and DAPI (blue). In the merged photos, the arrows indicate the

632 cell body. Scale bars, 20 μm.

633 PVN: paraventricular hypothalamic nucleus

634

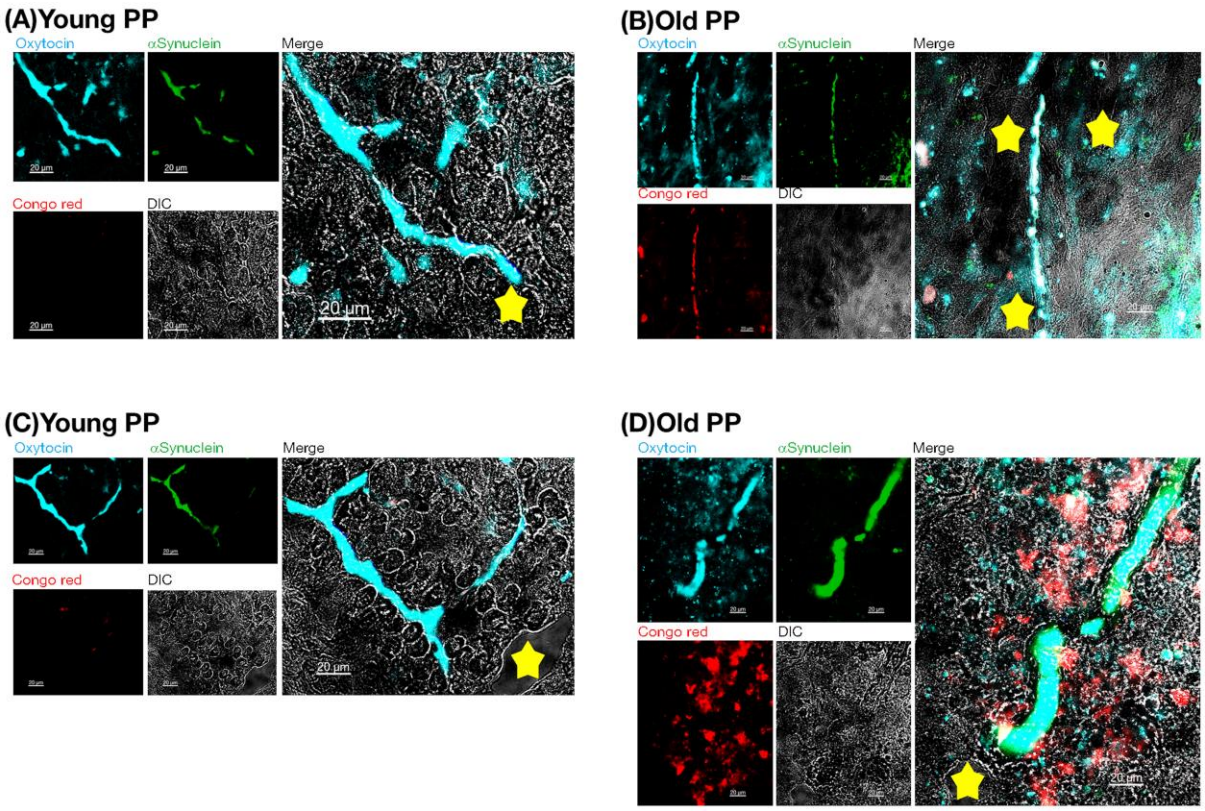

635

636 **Fig. 6.** Fluorescence photomicrographs of oxytocin, α-synuclein, and Congo red in the PP glands of

637 young and old bovines. Images were captured with laser confocal microscopy for oxytocin (light blue),

638 α-synuclein (green), Congo red (red), and DIC (gray). In the merged photos, the yellow stars indicate

639 the blood vessels. Scale bars, 20 μm.

640 PP: posterior pituitary

641 DIC: differential interference contrast

642

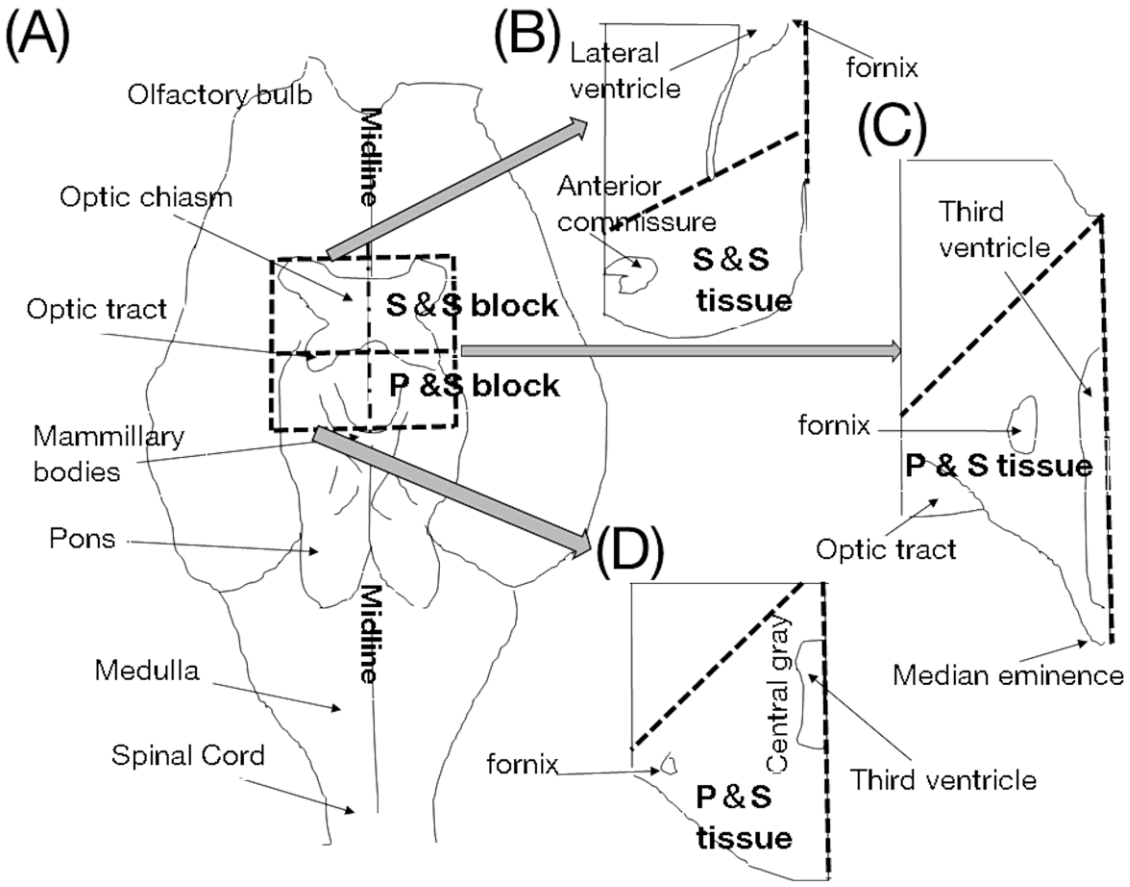

Supplementary Fig. 1. Schematic illustration of brain tissue sampling. Brain tissues were dissected as per the dotted line on the ventral side (A) with the following margins: rostrally-rostral border of the optic chiasm; caudally-rostral to the mammillary bodies; lateral to the optic chiasm; and 0.5 cm dorsal to the third ventricle. The block was then split into two parts by cutting from the rostral to the median eminence, yielding an anterior part containing the suprachiasmatic nucleus and supraoptic nucleus (S & S block) and a posterior part containing the paraventricular hypothalamic nucleus and supraoptic nucleus (P & S block). The blocks were further cut. Both the S & S and P & S blocks were cut at the midlines to obtain left and right sides. Using the bovine brain atlas (Graïc *et al.*, 2018; Okamura, 2002) as a reference, the blocks were further cut using their exterior shapes and the third or lateral ventricles as landmarks as the dotted line (B, C, D) to obtain tissue sample containing the suprachiasmatic nucleus and supraoptic nucleus (S & S tissue) and tissue containing the paraventricular hypothalamic nucleus and supraoptic nucleus (P & S tissue).

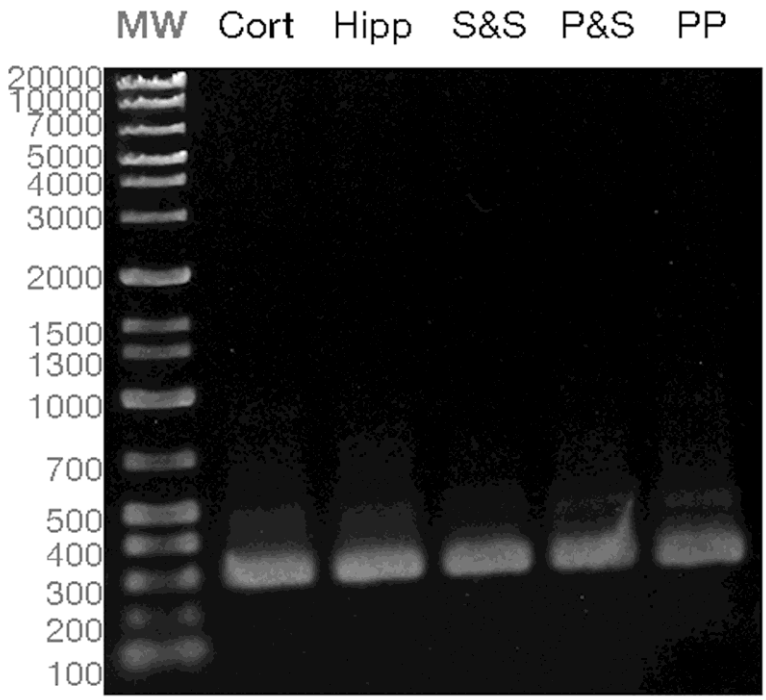

Supplementary Fig. 2. Detection of *α-synuclein* mRNA in bovine brain regions by RT-PCR. Electrophoresis of PCR-amplified DNA products using primers for *α-synuclein* and cDNA derived from the bovine cortex, hippocampus (Hipp), tissues containing the suprachiasmatic nucleus and supraoptic nucleus (S & S), paraventricular hypothalamic nucleus and supraoptic nucleus (P & S), or posterior pituitary (PP) tissues of post-pubertal heifers. The sizes of the obtained DNA products met expectations—303 bp. The marker lane (MW) indicates the DNA marker.

RT-PCR: reverse transcription-polymerase chain reaction.

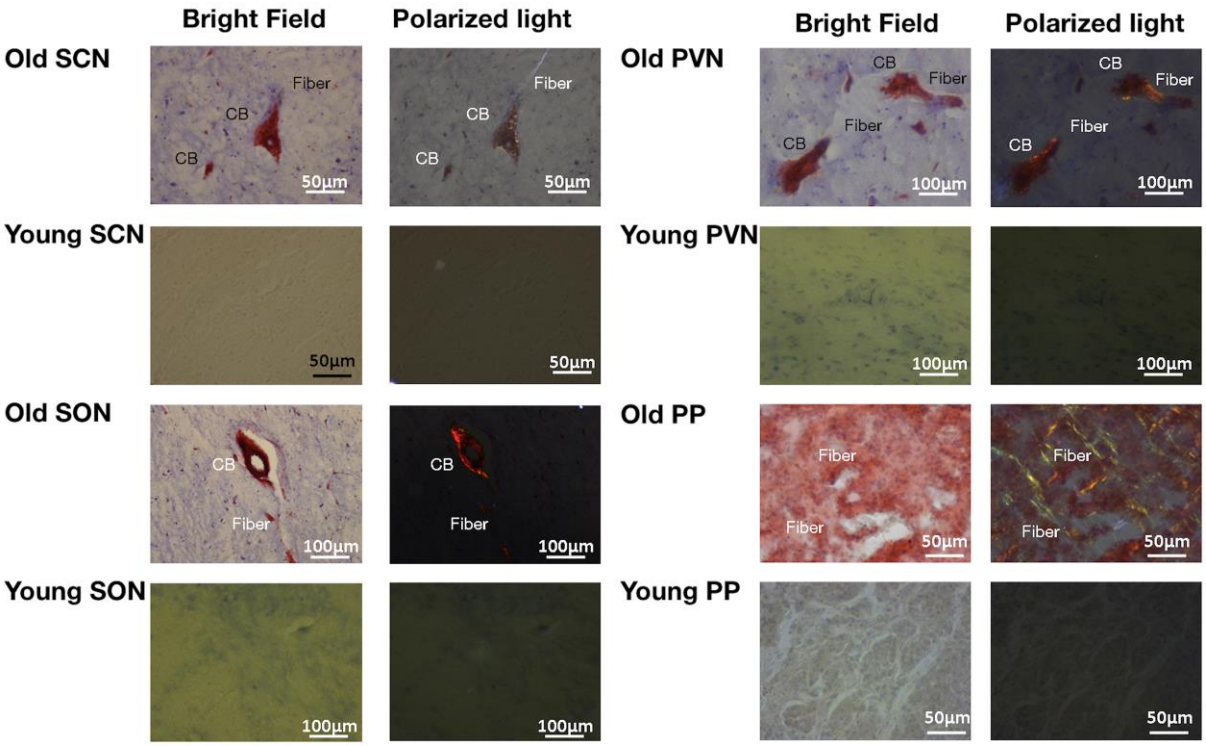

Supplementary Fig. 3. Congo red staining for amyloid deposit in SCN, SON, PVN, and PP in young and old bovines. The bright-field microscopy showed amyloid deposit regions in red. The polarized light microscopy results showed amyloid deposits in green or yellow. Scale bars are 50 μm in SCN and PP, and 100 μm in SON and PVN.

SCN: suprachiasmatic nucleus; SON: supraoptic nucleus; PVN: paraventricular hypothalamic nucleus; PP: posterior pituitary

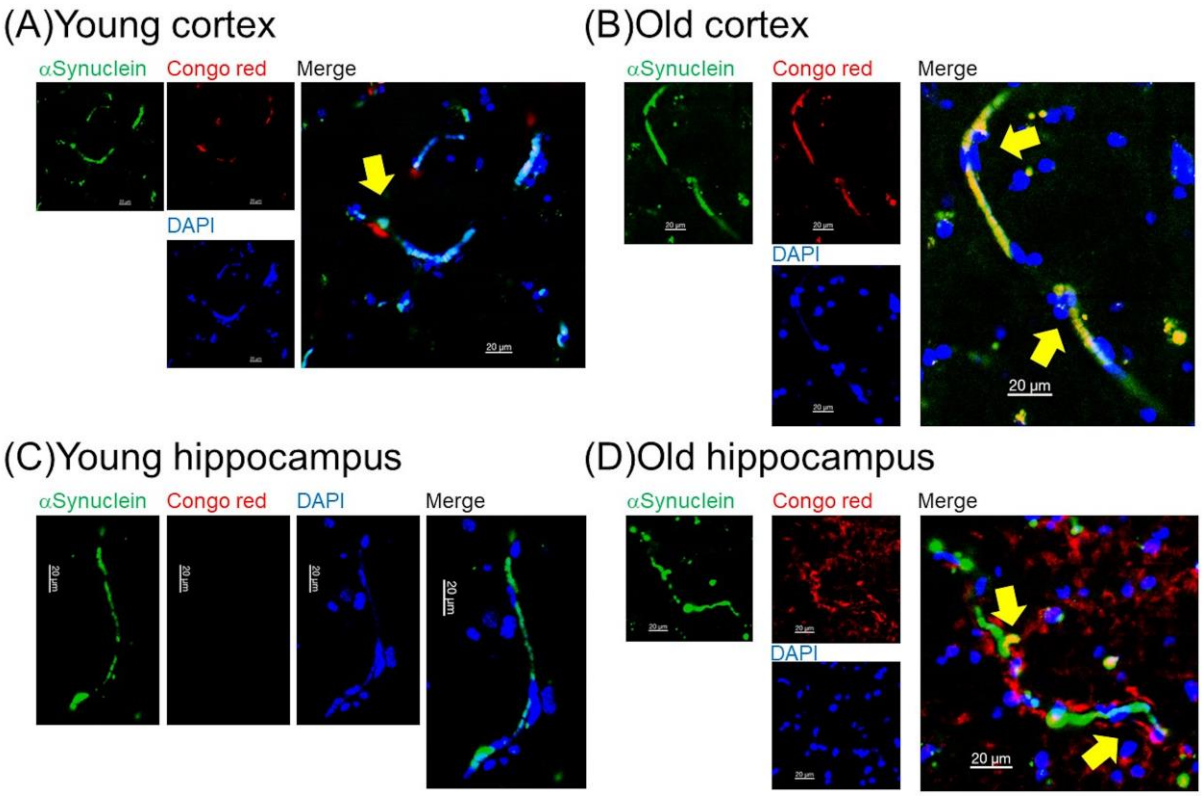

676

677

678 **Supplementary Fig. 4.** Fluorescence photomicrographs of α-synuclein, Congo red, and DAPI in the

679 cortex (A, B) and hippocampus (C, D) of young and old bovines. Images were captured with laser

680 confocal microscopy for a-synuclein (green), Congo red (red), and DAPI (blue). In the merged photos,

681 the yellow arrows indicate the co-localization of α-synuclein and Congo red in the cell body. Scale

682 bars, 20 μm.

683

684 **Supplementary Table 1.** Details of primers for bovine genes used for RT-PCR or quantitative RT-PCR
685

Gene	Primer sequence 5'-3'		Position		Size
Species			Nucleotide	Exon	(bp)
SNCA [a]	F	GACGCCGGGTGAGTGTG	18–34	1	303
	R	CAATGCTCCCTGCTCCTTCT	301–320	4	
SNCA[b]	F	GCCGGGTGAGTGTGGTGTA	21–39	1–2	80
	R	GACTCCCTCCTTGGCCTTTG	81–100	2	
YWHAZ [b]	F	AGACGGAAGGTGCTGAGAAA	256–275	2	123
	R	CGTTGGGGATCAAGAACTTT	359–378	3	
SDHA [b]	F	CATCCACTACATGACGGAGCA	428–448	5	90
	R	ATCTTGCCATCTTCAGTTCTGCTA	494–517	5	

686 RT-PCR, reverse transcription polymerase chain reaction; SNCA, synuclein alpha; SDHA, Succinate
687 dehydrogenase complex flavoprotein subunit A; YWHAZ, Tyrosine 3-Monooxygenase/Tryptophan 5-
688 Monooxygenase Activation Protein Zeta.

689 [a] For RT-PCR.

690 [b] For quantitative RT-PCR.

691

692 **Supplementary Table 2.** Mean ± SEM of the number of examined oxytocin -positive, α-synuclein-
693 positive, or Congo red-positive cell bodies and fibers in the suprachiasmatic nucleus (SCN),
694 supraoptic nucleus (SON), paraventricular hypothalamic nucleus (PVN), and posterior pituitary (PP)
695 gland of the young (n = 5) and old (n = 5) groups.

696 **Young group**

	Cell body in SCN/SON/PVN	Fiber in SCN/SON/PVN	Fiber in PP
Oxytocin+	40.0 ± 0.5	37.4 ± 0.7	37.4 ± 0.7
α-synuclein+	52.8 ± 0.7	50.6 ± 0.8	43.6 ± 2.5
Congo red+	4.8 ± 1.8	1.6 ± 0.2	13.8 ± 3.0

697 **Old group**

	Cell body in SCN/SON/PVN	Fiber in SCN/SON/PVN	Fiber in PP
Oxytocin+	32.6 ± 0.7	31.2 ± 0.6	28.2 ± 1.1
α–synuclein+	59.4 ± 1.7	50.8 ± 0.7	48.6 ± 3.2
Congo red+	60.0 ± 1.8	50.4 ± 0.7	48.4 ± 3.0

698

699

Supplementary Table 3. Mean ± SEM of the percentage of oxytocin cell bodies or fibers that co-localize α-synuclein or Congo red and the percentage of α-synuclein or Congo red cells that co-localize oxytocin in the young (n = 5) and old (n = 5) SCN, SON, PVN, and PP tissues.

(A) Cell body in the SCN /SON/PVN

	Young	Old	P-value
Oxytocin cells co-localize α-synuclein	52.6 ± 1.6	99.4 ± 0.6	< 0.01
Oxytocin cells co-localize Congo red	9.2 ± 4.7	98.7 ± 0.8	< 0.01
Oxytocin cells co-localize both	3.8 ± 1.8	98.7 ± 0.8	< 0.01
α-synuclein cells co-localize oxytocin	39.8 ± 1.0	54.8 ± 2.2	<0.01
Congo red cells co-localize oxytocin	70.0 ± 6.8	53.9 ± 2.4	NS

(B) Fibers in the SCN /SON/PVN.

	Young	Old	P-value
Oxytocin cells co-localize α-synuclein	54.6 ± 1.2	96.9 ± 1.4	< 0.01
Oxytocin cells co-localize Congo red	1.6 ± 0.7	94.9 ± 2.1	< 0.01
Oxytocin cells co-localize both	0.6 ± 0.2	94.9 ± 2.1	< 0.01
α-synuclein cells co-localize oxytocin	40.3 ± 0.6	59.5 ± 0.7	< 0.01
Congo red cells co-localize oxytocin	30.0 ± 12.2	58.7 ± 1.0	NS

(C) Fibers in the PP.

	Young	Old	P-value
Oxytocin cells co-localize α-synuclein	54.6 ± 1.2	98.6 ± 0.9	< 0.01
Oxytocin cells co-localize Congo red	7.3 ± 5.3	98.6 ± 0.9	< 0.01
Oxytocin cells co-localize both	2.8 ± 2.1	91.9 ± 2.7	< 0.01

α-synuclein cells co-localize oxytocin	47.3 ± 2.5	57.7 ± 2.2	< 0.05
Congo red cells co-localize oxytocin	28.0 ±15.5	57.8 ± 1.6	NS

708

709

710